Volume 18, Number 1, 2025. pp. 41-48

Jordan Journal of Physics

ARTICLE

Negative Ion Formation in H + H Collisions at Low- to High-Energies

Saed J. Al Atawneh

Department of Physics, Zarqa University, Zarqa 13110, Jordan.

Doi: **https://doi.org/10.47011/18.1.5**

Received on: 03/07/2023; *Accepted on: 09/10/2023*

Abstract: For various branches of science, it is essential to determine all possible reactions and collisional cross-sections. Despite extensive large-scale studies conducted over the past decades to provide such data, many fundamental atomic and molecular cross-section values remain unknown, and the accuracy of the available data still requires verification.

In this paper, we present cross-section calculations for negative ion formation (ion-pair formation) in hydrogen-hydrogen atom collisions based on the classical trajectory and quasi-classical trajectory Monte Carlo models. By comparing our results with available experimental data and theoretical predictions, we find that the QCTMC calculations align well with previous studies. However, the negative ion formation cross-sections obtained using the CTMC model underestimate all previously reported theoretical and experimental values. Nonetheless, the CTMC results show good agreement with the *Q*-, *P*-series approximation in the energy range of 1–10 keV. We present negative ion formation cross-sections for impact energies ranging from 1 keV to 100 keV, which are relevant to applications in astronomy, atmospheric sciences, plasma laboratories, and fusion research.

Keywords: Atom-atom collision, Negative ion formation, Classical Trajectory Monte Carlo method, Quasi-classical Trajectory Monte Carlo method.

1. Introduction

Recently, the search for new energy sources has become increasingly urgent [1]. In contrast to nuclear fission energy, which creates massive amounts of nuclear waste that are damaging to the environment and humans [2], the current tendency is to employ clean fusion energy, which does not release or leave any dangerous radioactive material [1]. Therefore, the development of nuclear fusion reactors such as tokamak has attracted attention as a clean energy source [3, 4].

In fusion reactors, the limiter and divertor regions contain plenty of neutrals, such as hydrogen atoms [5-8]. These regions, characterized by lower temperatures and high particle densities, serve as sites for numerous atomic, ionic, and molecular collisions [5–8]. Plasma-neutral interactions involving hydrogen play a crucial role in plasma diagnostics, as the cross-sections of elastic and inelastic collisions provide essential data for diagnostic tools such as Beam Emission Spectroscopy (BES) [5–10]. Consequently, many studies have focused on plasma-neutral interactions in divertor and limiter regions [5–18].

In this study, we investigate the cross-sections of negative ions formation (ion-pair formation) resulting from collisions between ions and atoms or between two atoms. Specifically, we examine the production of negative ions in collisions between two ground-state hydrogen atoms over an energy range of 1 keV to 100 keV. These cross sections are not only fundamental to fusion research but also play

Corresponding Author: Saed J. Al Atawneh **Email**: salatawneh@zu.edu.jo

a significant role in energy balance studies in astrophysics [19] and atmospheric sciences [20].

Negative ions also play an essential role in various industries, including their application in etching processes (NBIs) [21]. Even in biological sciences, negative ions play an essential role as antioxidants against free radicals that are hazardous to the human body. However, no significant efforts have been made to coordinate experiments and theory, basic science, and applications to understand the structure and formation dynamics of negative ions.

In this study, we are specifically interested in ion-pair cross-sections in atom-atom collisions, as described by:

$$H + H \rightarrow H^{+} + H^{-} \quad (1)$$

The four-body classical (CTMC) and quasi-classical (QCTMC) Monte Carlo simulations were performed [5-15] to calculate the negative ion formation cross-sections. The QCTMC is just a modified version of the standard model that adds a quantum feature to the model potential, such as the Heisenberg correction term to the pure Coulomb inter-particle potential. This modification accounts for nonclassical effects, enhancing the stability of classical hydrogen atoms [22, 23]. In traditional CTMC simulations, the absence of lower energy bounds imposed by quantum mechanics often leads to autoionization or collapse of classical hydrogen atoms, potentially affecting the accuracy of cross-section calculations.

In this work, we present cross-section data for negative ion formation obtained using both the standard and modified CTMC methods. To the best of our knowledge, such data have not been previously reported. Our calculations span an energy range of 1 to 100 keV, which is particularly relevant to applications in astronomy, atmospheric sciences, plasma laboratories, and fusion research. Unless otherwise stated, all results are presented in atomic units.

2. Theory

2.1. The CTMC Models

As is well-known, classical descriptions of collision processes work extremely well [5-10, 16-18]. In this model, the H atom is represented by two particles: the ionic core of H and one active electron. All particles can be described by their masses and charges [9, 23]. Let P represent the ionic core of the projectile, P_e the electron of the projectile, T the ionic core of the target, and T_e the electron of the target [9]. Interactions between electrons are explicitly included in our four-body calculations. At time $\boldsymbol{t} = -\infty$, we assume that the four-body collision system is made up of two isolated atoms: a projectile atom (P, P_e), marked as particles (1, 4), and a target atom (T, T_e), marked as particles (2, 3), as shown in Fig. 1 [8]. At the beginning, both particles are in the ground state (nl=*1, 0*) [8]. We used the Coulomb potential to describe all interactions [8, 9]. Figure 1 depicts the relative position vectors for the four-body collision systems.

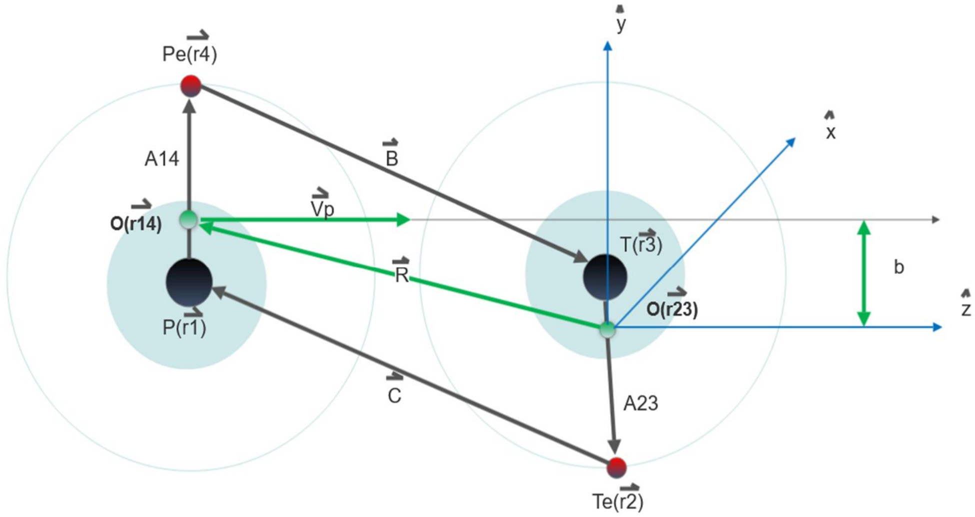

FIG. 1. The schematic diagram represents the relative position vectors for particles involved in our 4-body collision systems. $\vec{A}_{14} = \vec{r}_4 - \vec{r}_1, \vec{B} = \vec{r}_4 - \vec{r}_3, \vec{A}_{23} = \vec{r}_3 - \vec{r}_2$, and $\vec{C} = \vec{r}_2 - \vec{r}_1$, in such way that $\vec{A}_{14} + \vec{A}_{23} + \vec{B} + \vec{C} = 0$. Where $O(\vec{r}_{14})$ and $O(\vec{r}_{23})$ represent centre-of-mass vectors for target and projectile systems respectively, with b as their impact parameter.

The initial electronic states can be determined by means of a microcanonical distribution. A microcanonical set represents the initial state of the target and projectile, compelled by their binding energy in any given shell, and can be described as follows:

$$\rho_{E_0}(\vec{A},\dot{\vec{A}}) = K_1\delta(E_0 - E) = \delta\left(E_0 - \frac{1}{2}\mu_{T,Te,P,Pe}\dot{\vec{A}}^2 - V(A)\right). \quad (2)$$

Here, K_1 is a normalization constant, E_0 is the ionization energy of the active electron, $V(A)$ represents the electron and ionic-core potential, A is the length of the vector $\vec{A}$, and μ_{T,T_eP,P_e} is the reduced mass of particles ("T", "T_e", "P", and "P_e") [5-10]. According to Eq. (2), the electronic coordinates are restricted within intervals where Eq. (3) holds:

$$\frac{1}{2}\mu_{Te}\dot{\vec{A}} = E_0 - V(A) > 0\,. \quad (3)$$

Hamilton equation is given by:

$$H_0 = T + V_{coul}, \quad (4)$$

where

$$T = \frac{\vec{P}_p^2}{2m_p} + \frac{\vec{P}_{pe}^2}{2m_{pe}} + \frac{\vec{P}_T^2}{2m_T} + \frac{\vec{P}_{Te}^2}{2m_{Te}}, \quad (5)$$

and

$$V_{coul} = \frac{Z_p Z_{Pe}}{|\vec{r}_p-\vec{r}_{Pe}|} + \frac{Z_P Z_T}{|\vec{r}_P-\vec{r}_T|} + \frac{Z_p Z_{Te}}{|\vec{r}_p-\vec{r}_{Te}|} + \frac{Z_{pe} Z_T}{|\vec{r}_{pe}-\vec{r}_T|} + \frac{Z_{Pe} Z_{Te}}{|\vec{r}_{pe}-\vec{r}_{Te}|} + \frac{Z_T Z_{Te}}{|\vec{r}_T-\vec{r}_{Te}|}. \quad (6)$$

Here, T and V_{coul} stand for total kinetic energy and Coulomb potential term, respectively [5-10]. $\vec{P}$, Z, $\vec{r}$, and m stand for momentum vector, charge, position vector, and mass of each particle, respectively [5-10]. Here are the equations of motion according to Hamiltonian mechanics:

$$\dot{\vec{P}}_p = -\frac{\delta H_0}{\delta \vec{r}_P} = \frac{Z_P Z_{Pe}}{|\vec{r}_p-\vec{r}_{Pe}|^3}(\vec{r}_P - \vec{r}_{Pe}) + \frac{Z_P Z_T}{|\vec{r}_P-\vec{r}_T|^3}(\vec{r}_P - \vec{r}_T) + \frac{Z_P Z_{Te}}{|\vec{r}_P-\vec{r}_{Te}|^3}(\vec{r}_P - \vec{r}_{Te}), \quad (7)$$

$$\dot{\vec{P}}_{Pe} = -\frac{\delta H_0}{\delta \vec{r}_{Pe}} = -\frac{Z_P Z_{Pe}}{|\vec{r}_P-\vec{r}_{Pe}|^3}(\vec{r}_P - \vec{r}_{Pe}) - \frac{Z_T Z_{Pe}}{|\vec{r}_T-\vec{r}_{Pe}|^3}(\vec{r}_T - \vec{r}_{Pe}) - \frac{Z_{Te} Z_{Pe}}{|\vec{r}_{Te}-\vec{r}_{Pe}|^3}(\vec{r}_{Te} - \vec{r}_{Pe}), \quad (8)$$

$$\dot{\vec{P}}_T = -\frac{\delta H_{H_0}}{\delta \vec{r}_T} = -\frac{Z_P Z_T}{|\vec{r}_P-\vec{r}_T|^3}(\vec{r}_P - \vec{r}_T) - \frac{Z_{Te} Z_T}{|Te-\vec{r}_T|^3}(\vec{r}_{Te} - \vec{r}_T) + \frac{Z_T Z_{Pe}}{|\vec{r}_T-\vec{r}_{Pe}|^3}(\vec{r}_T - \vec{r}_{Pe}), \quad (9)$$

$$\dot{\vec{P}}_{Te} = -\frac{\delta H_{H_0}}{\delta \vec{r}_{Te}} = -\frac{Z_P Z_{Te}}{|\vec{r}_P-\vec{r}_{Te}|^3}(\vec{r}_P - \vec{r}_{Te}) - \frac{Z_{Te} Z_T}{|Te-\vec{r}_T|^3}(\vec{r}_{Te} - \vec{r}_T) - \frac{Z_{Te} Z_{Pe}}{|\vec{r}_{Te}-\vec{r}_{Pe}|^3}(\vec{r}_{Te} - \vec{r}_{Pe}). \quad (10)$$

The Runge-Kutta method is typically utilized to numerically integrate equations of motion using an ensemble of approximately 5 × 10^6 primary trajectories per energy [5-10]. Such an ensemble typically is required in order to ensure statistical uncertainties of less than 5% [5-10]. The negative ion formation cross-section is given by:

$$\sigma = \frac{2\pi b_{max}}{N}\sum_j b_j, \quad (11)$$

where b_j is the impact parameter corresponding to the trajectory associated with a negative ion formation process, N is the total number of calculated trajectories, and b_{max} is the maximum value for the impact parameter where the described processes can occur. The statistical uncertainty of the cross-section can be calculated by:

$$\Delta\sigma = \sigma\left[\frac{N-N_P}{N\,N_P}\right]^{1/2}. \quad (12)$$

Here, N_P is the number of trajectories that satisfy the criteria for the negative ion formation process.

2.2. The QCTMC Model

The QCTMC model improves on the CTMC model by including a quantum correction term [6, 9, 10, 22, 23]. To simulate the Heisenberg uncertainty and Pauli principle, a modified Hamiltonian effective potential (V_H for Heisenberg and V_P for Pauli) is added to the pure Coulomb inter-particle potentials to represent a non-classical effect [22, 23]. As a result, inter-particle interactions are enhanced. Thus:

$$H_{QCTMC} = H_0 + V_H + V_P, \quad (13)$$

where H_0 is the standard Hamiltonian [see Eq. (4)], and the correction terms for H_0 include:

$$V_H = \sum_{i=1}^{N}\frac{1}{mr_i^2}f\left(\vec{r}_i,\vec{p}_i;\xi_H;\alpha_H\right), \quad (14)$$

and

$$V_p = \sum_{i=1}^{N}\sum_{j=i+1}^{N}\frac{2}{mr_{ij}^2}f\left(\vec{r}_{ij},\vec{p}_{ij};\xi_p;\alpha_p\right)\delta_{s_i,s_j}. \quad (15)$$

Here, i and j refer to the electron indices. Additionally, $r_{ij} = r_j - r_i$, and the relative momentum is determined as follows:

$$\vec{P}_{ij} = \frac{m_i\vec{p}_j - m_j\vec{p}_i}{m_i + m_j}, \tag{16}$$

where $\delta_{s_i,s_j} = 1$ if the ith and jth electrons have the same spin, and 0 if they are different [9, 10]. Finally, the constraining potential is chosen as:

$$f(\vec{r}_{\lambda\nu}, \vec{p}_{\lambda\nu}; \xi, \alpha) = \frac{\xi^2}{4\alpha r_{\lambda\nu}^2 \mu_{\lambda\nu}} exp\left\{\alpha\left[1 - \left(\frac{\vec{r}_{\lambda\nu}\vec{p}_{\lambda\nu}}{\xi}\right)^4\right]\right\}. \tag{17}$$

Since a hydrogen atom consists of one electron and one proton, Heisenberg constraints with a specific scale parameter, a hardness parameter ($\boldsymbol{\alpha_H}$ = 3.0), and a dimensionless constant ($\boldsymbol{\xi_H}$ = 0.9258) are applied to the four-body QCTMC model. As illustrated in the following equation:

$$f(\vec{r}_{T,Te}, \vec{P}_{T,Te}; \varepsilon_H, \alpha_H) = \frac{{\xi_H}^2}{4\alpha_H \vec{r}_{T,Te}^2 \mu_{T,Te}} exp\left\{\alpha_H\left[1 - \left(\frac{\vec{r}_{T,Te}\vec{P}_{T,Te}}{\xi_H}\right)^4\right]\right\}. \tag{18}$$

Similar to the target atom, the correction term should also be added to the projectile atom as follows:

$$f(\vec{r}_{P,Pe}, \vec{P}_{P,Pe}; \varepsilon_H, \alpha_H) = \frac{{\xi_H}^2}{4\alpha_H \vec{r}_{P,Pe}^2 \mu_{P,Pe}} exp\left\{\alpha_H\left[1 - \left(\frac{\vec{r}_{P,Pe}\vec{P}_{P,Pe}}{\xi_H}\right)^4\right]\right\}. \tag{19}$$

As shown in Fig. 1, the equations of motion, which incorporate Hamiltonian mechanics as well as correction terms for cross-section calculations, can be expressed as:

$$\dot{\vec{P}}_p = -\frac{\delta H_{QCTMC}}{\delta \vec{r}_P} = \left[\frac{Z_P Z_{Pe}}{|\vec{r}_p - \vec{r}_{Pe}|^3}(\vec{r}_P - \vec{r}_{Pe}) - \left(-\frac{{\xi_H}^2}{2\alpha_H \vec{r}_{P,Pe}^4 \mu_{P,Pe}} - \frac{(\vec{P}_{P,Pe})^4}{\mu_{P,Pe}{\xi_H}^2}\right) exp\left\{\alpha_H\left[1 - \left(\frac{r_{P,Pe}P_{P,Pe}}{\xi_H}\right)^4\right]\right\}\right] + \frac{Z_P Z_T}{|\vec{r}_P - \vec{r}_T|^3}(\vec{r}_P - \vec{r}_T) + \frac{Z_P Z_{Te}}{|\vec{r}_P - \vec{r}_{Te}|^3}(\vec{r}_P - \vec{r}_{Te}), \tag{20}$$

$$\dot{\vec{P}}_{Pe} = -\frac{\delta H_{QCTMC}}{\delta \vec{r}_{Pe}} = -\left[\frac{Z_P Z_{Pe}}{|\vec{r}_P - \vec{r}_{Pe}|^3}(\vec{r}_P - \vec{r}_{Pe}) + \left(-\frac{{\xi_H}^2}{2\alpha_H \vec{r}_{P,Pe}^4 \mu_{P,Pe}} - \frac{(\vec{P}_{P,Pe})^4}{\mu_{P,Pe}{\xi_H}^2}\right) exp\left\{\alpha_H\left[1 - \left(\frac{r_{P,Pe}P_{P,Pe}}{\xi_H}\right)^4\right]\right\}\right] - \frac{Z_T Z_{Pe}}{|\vec{r}_T - \vec{r}_{Pe}|^3}(\vec{r}_T - \vec{r}_{Pe}) - \left[\frac{Z_{Te}Z_{Pe}}{|\vec{r}_{Te} - \vec{r}_{Pe}|^3}(\vec{r}_{Te} - \vec{r}_{Pe}) - \left(-\frac{{\xi_P}^2}{2\alpha_P \vec{r}_{Te,Pe}^4 \mu_{Te,Pe}} - \frac{(\vec{P}_{Te,Pe})^4}{\mu_{Te,Pe}{\xi_H}^2}\right) exp\left\{\alpha_p\left[1 - \left(\frac{r_{Te,Pe}P_{Te,Pe}}{\xi_P}\right)^4\right]\right\}\right], \tag{21}$$

$$\dot{\vec{P}}_T = -\frac{\delta H_{QCTMC}}{\delta \vec{r}_T} = -\frac{Z_P Z_T}{|\vec{r}_P - \vec{r}_T|^3}(\vec{r}_P - \vec{r}_T) - \left[\frac{Z_{Te}Z_T}{|Te - \vec{r}_T|^3}(\vec{r}_{Te} - \vec{r}_T) + \left(-\frac{{\xi_H}^2}{2\alpha_H \vec{r}_{T,Te}^4 \mu_{T,Te}} - \frac{{\vec{P}_{T,Te}}^4}{\mu_{T,Te}{\xi_H}^2}\right) exp\left\{\alpha_H\left[1 - \left(\frac{r_{T,Te}P_{T,Te}}{\xi_H}\right)^4\right]\right\}\right] + \frac{Z_T Z_{Pe}}{|\vec{r}_T - \vec{r}_{Pe}|^3}(\vec{r}_T - \vec{r}_{Pe}), \tag{22}$$

$$\dot{\vec{P}}_{Te} = -\frac{\delta H_{QCTMC}}{\delta \vec{r}_{Te}} = -\frac{Z_P Z_{Te}}{|\vec{r}_P - \vec{r}_{Te}|^3}(\vec{r}_P - \vec{r}_{Te}) - \left[\frac{Z_{Te}Z_T}{|Te - \vec{r}_T|^3}(\vec{r}_{Te} - \vec{r}_T) + \left(-\frac{{\xi_H}^2}{2\alpha_H \vec{r}_{T,Te}^4 \mu_{T,Te}} - \frac{{\vec{P}_{T,Te}}^4}{\mu_{T,Te}{\xi_H}^2}\right) exp\left\{\alpha_H\left[1 - \left(\frac{r_{T,Te}P_{T,Te}}{\xi_H}\right)^4\right]\right\}\right] - \left[\frac{Z_{Te}Z_{Pe}}{|\vec{r}_{Te} - \vec{r}_{Pe}|^3}(\vec{r}_{Te} - \vec{r}_{Pe}) - \left(-\frac{{\xi_P}^2}{2\alpha_P \vec{r}_{Te,Pe}^4 \mu_{Te,Pe}} - \frac{(\vec{P}_{Te,Pe})^4}{\mu_{Te,Pe}{\xi_H}^2}\right) exp\left\{\alpha_p\left[1 - \left(\frac{r_{Te,Pe}P_{Te,Pe}}{\xi_P}\right)^4\right]\right\}\right]. \tag{23}$$

3. Results and Discussion

Despite the importance of negative ion production in several scientific fields, no substantial efforts have been made to coordinate experiments and theories, fundamental science, and applications to better understand the structure and formation dynamics of negative ions. In the present paper, the production of negative ions can be described qualitatively using a simple kinematics picture as follows: A second electron approaches a hydrogen atom, which consists of a proton and an electron. The electric field of the second electron (which decreases with distance as r^{-2}) creates a dipole moment in the neutral hydrogen atom, and then. As a result, the two electrons position themselves on opposite sides of the proton, forming a stable negative ion, as illustrated in Fig. 2.

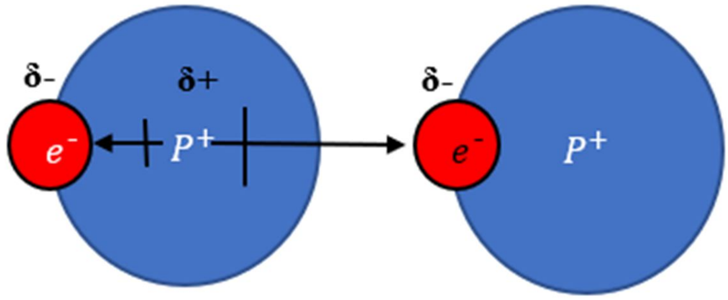

FIG. 2. The dipole moment induced by the second electron in H+H collisions.

The induced dipole moment is proportional to the polarizing electron's electric field and, consequently, to r^{-2}. The second electron is now surrounded by the electric field of the dipole it has created in the neutral H atom, allowing it to be captured. In general, the initial stage of the negative ion formation process is governed by a weak polarization interaction between two neutral species, exhibiting a relatively weak dependence on the interatomic distance (R). In contrast, the final ion-pair formation stage is strongly dominated by Coulomb interactions, which scale as 1/R.

Classically, the negative ion formation channel can be categorized into two channels. The first is the target capture channel, as described by Eq. (24):

$$H_P + H_T \rightarrow H_P^+ + H_T^- \qquad (24)$$

The second is the projectile capture channel, as represented by Eq. (25):

$$H_P + H_T \rightarrow H_P^- + H_T^+ \qquad (25)$$

As discussed in previous reviews [5, 9], the collision system (H+H) is symmetrical. Consequently, the negative ion formation cross-section in this study is identical for both the target and projectile atoms.

Figure 3 illustrates the probability of negative ion formation, as determined by CTMC and QCTMC computational approaches, as a function of the impact parameter for projectile impact energies of 20, 60, and 100 keV. The probability distributions were fitted using Gaussian functions, with the peak maxima also shown in Fig. 3. Significant variations in the peak maxima were observed, with lower impact energies corresponding to higher maximum values of the impact parameter.

This behavior can be understood using a simple kinematic picture: at low impact energies, the projectile remains in close proximity to the target for an extended period during the collision, increasing the likelihood of negative ion formation due to prolonged interactions among ionic cores and electrons (slow-collision scenario). This suggests that as the impact parameter increases, the probability of negative ion formation also rises [7, 8].

Conversely, at higher impact energies, the probability of negative ion formation is inversely proportional to the impact parameter. This indicates that negative ion formation predominantly occurs in short-range (close) collisions. The impact parameter analysis in Fig. 3 confirms this, showing that projectiles with higher impact energies exhibit a much narrower impact parameter range compared to those with lower impact energies.

Once again, this underscores that the underlying mechanism of negative ion formation is governed by weak polarization interactions between two neutral atoms. Similar to the CTMC results, the probability of negative ion formation as a function of the impact parameter in the QCTMC model follows the same trend (see Fig. 3). However, the QCTMC calculations predict systematically higher probabilities than the standard CTMC model, emphasizing the significance of the Heisenberg correction term.

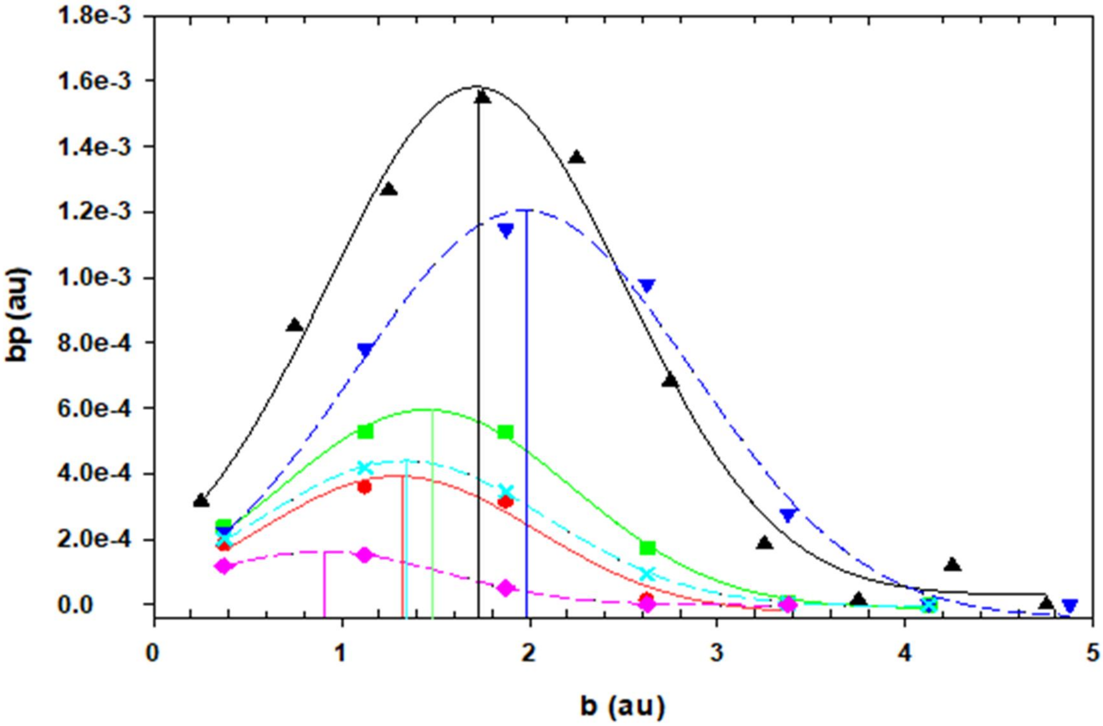

FIG. 3. Negative ion formation probability in H+H collisions using the CTMC and QCTMC methods as a function of impact parameters. Blue triangles down: the CTMC results for 20 keV. Cyan crosses: the CTMC results for 60 keV. Pink diamonds: the CTMC results for 100 keV. Black triangles up: the QCTMC results for 20 keV. Green squares: the QCTMC results for 60 keV. Red circles: the QCTMC results for 100 keV.

Figure 4 displays the cross-sections of present negative ion formation in H+H collisions as a function of impact energy, along with the experimental data from Gealy and Van Zyl [24] and McClure [25]. Figure 4 also displays the earlier theoretical cross-section results from Ovchinnikov [26], who showed a mechanism for the formation of negative ions in the slow-collision regime using a Q-,P-series method. Q-,P-series establishes a connection between the ground singlet H + H state and the ground $\mathrm{H}^{+} + \mathrm{H}^{-}$ state. As noted, the findings of Gealy and Van Zyl [24] at low energies below 1 keV are somewhat inconsistent with previous and contemporary studies. The present QCTMC results for negative ion formation cross sections in the energy range of 1 keV to 20 keV are in excellent agreement with the experimental and theoretical data of McClure [25] and Ovchinnikov [26]. In contrast, the current CTMC approaches underestimate all prior theoretical and experimental results. Additionally, in the high-energy range above 80 keV, when the projectile's energy (velocity) exceeds that of an orbital electron veleocity ($v_p \gg v_e$), the Heisenberg correction component is minimal (see Fig. 4). This means that the CTMC and QCTMC calculations yield roughly similar results, which can be explained by two factors: 1) The Heisenberg potential has less influence as the projectile momentum increases, and 2) The Heisenberg potential is inversely proportional to the square of the relative distance between colliders ($V_H \; \alpha \; {}^{1}\!/_{r_{ij}^{2}}$), see Eq. (17). As a result, the $V_H(r,p,\alpha)$ potential contributes in the low-to-medium energy region but is negligible in the high-energy region.

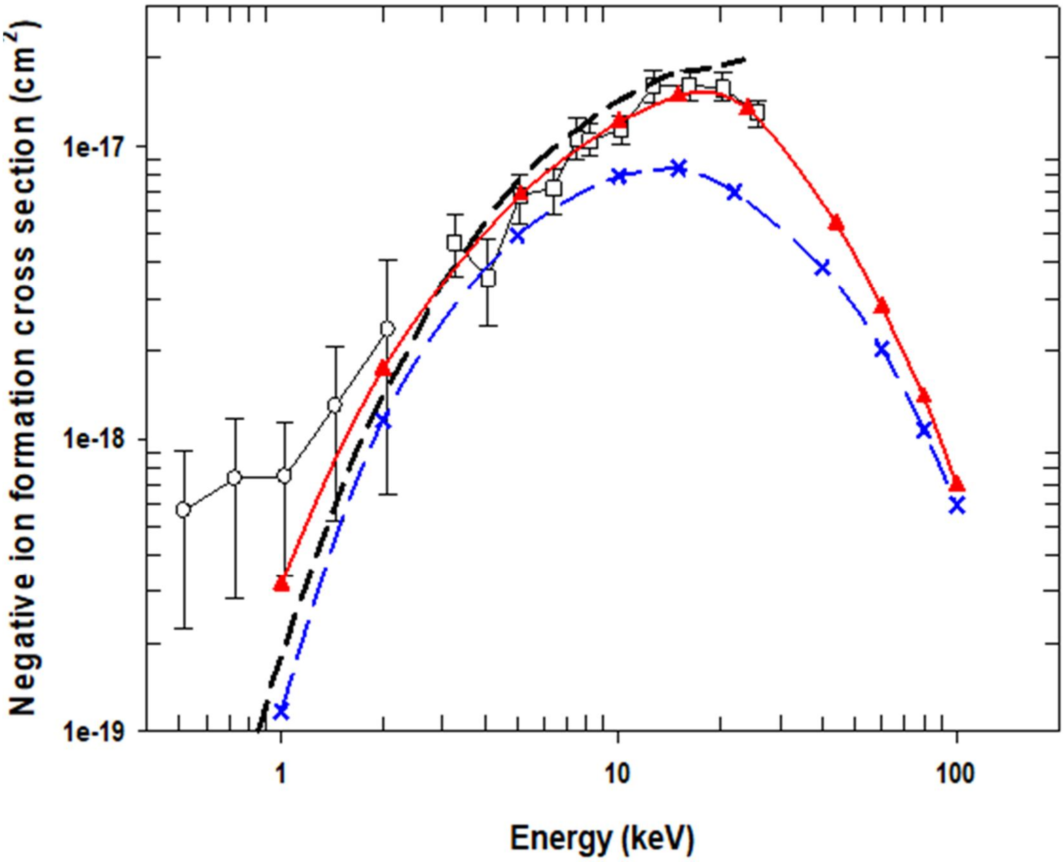

FIG. 4. Negative ion formation cross-section in H+H collision as a function of impact energy. Red triangles-solid line: presents QCTMC results. Blue crosses-dashed line: presents CTMC results. Open circles-solid line: measured data by Gealy and Van Zyl [24]. Open squares-solid line: measured data by McClure [25]. Black dashed line: Q-, P-series results by Ovchinnikov *et al*. [26].

4. Conclusion

We have presented negative ion formation cross-sections for H+H collisions using both four-body CTMC and four-body QCTMC calculation methods. Our calculations were performed for impact energies ranging from 1 to 100 keV, where the cross sections are expected to be significant to astronomy, atmospheric sciences, plasma laboratories, and fusion research. We found a consistent pattern in the maximum impact parameter for negative ion formation probability as a function of impact energy in both the CTMC and QCTMC approaches. Specifically, the maximum impact parameter was found to be larger at lower energies. Furthermore, the QCTMC results showed good agreement with previously reported experimental and theoretical data. In contrast, our CTMC calculations slightly underestimated previous results. However, at impact energies between 1 and 10 keV, the CTMC data aligned well with *Q*- and *P*-series approximation data. In conclusion, we found that the QCTMC approach accurately calculates the cross-sections of negative ion formation.

Acknowledgment

This work has no funding.

References

[1] Dunlap, R.A., "Energy from Nuclear Fusion" (IOP Publishing, 2021).

[2] Tikhomirov, G.V. and Gerasimov, A.S., J. Phys. Conf. Ser., 1689 (1) (2020) 012032.

[3] Ikeda, K., Nucl. Fusion, 47 (6) (2007) E01.

[4] Janev, R.K., Langer, W.D., Evans, K., and Post, D.E., "Atomic and Molecular Processes in Hydrogen–Helium Plasma" (Springer-Verlag, Berlin, 1985).

[5] Atawneh, S.J.A., Asztalos, Ö., Szondy, B., Pokol, G.I., and Tőkési, K., Atoms, 8 (2020) 31.

[6] Atawneh, S.J.A. and Tőkési, K., Atomic Data Nucl. Data, 146 (2022) 101513.

[7] Atawneh, S.J.A. and Tőkési, K., J. Phys. B: At. Mol. Opt. Phys., 54 (2021) 065202.

[8] Atawneh, S.J.A., PhD dissertation, Debrecen U, ProQuest, http://hdl.handle.net/2437/329082.

[9] Atawneh, S.J.A. and Tőkési, K., Phys. Chem. Chem. Phys., 24 (2022) 15280.

[10] Atawneh, S.J.A. and Tőkési, K., Nucl. Fusion., 62 (2021) 026009.

[11] Shipsey, E.J., Browne, J.C., and Olson, R.E, J. Phys. B: At. Mol. Opt. Phys., 14 (1981) 869.

[12] McCullough, R.W., Phys. Scr., T92 (2001) 76.

[13] Olson, R.E., Reinhold, C.O., and Schultz, D.R., Proc. 4th Workshop on High-Energy Ion-Atom Collision Processes, Debrecen, Hungary (1990).

[14] Abrines, R. and Percival, I.C., Proc. Phys. Soc., 88 (1966) 861.

[15] Janev, R.K. and McDowell, M.R.C., Phys. Lett. A, 102 (1984) 405.

[16] Velayati, A. and Ghanbari-Adivi, E., Eur. Phys. J. D, 72 (2018) 100.

[17] Velayati, A., Ghanbari-Adivi, E., and Ghorbani, O., J. Phys. B: At. Mol. Opt. Phys., 51 (2018) 185201.

[18] Ghavaminia, H. and Ghanbari-Adivi, E., Chinese Phys. B, 24 (2015) 073401.

[19] Hartquist, T.W., "Molecular Astrophysics" (Cambridge University Press, 1994).

[20] Wayne, R.P., "Atmospheric Chemistry" (Oxford University Press, 1991).

[21] Makabe, T. and Petrovic, Z.L., Appl. Surf. Sci., 192 (2002) 88.

[22] Wilets, L. and Cohen, J.S., Cont. Phys., 39 (1998) 163.

[23] Kirschbaum, C.L. and Wilets, L., Phys. Rev. A, 21 (1980) 834.

[24] Gealy, M.W. and Zyl, B.V., Phys. Rev. A, 36 (1987) 3100.

[25] McClure, G.W., Phys. Rev., 166 (1968) 22.

[26] Yu Ovchinnikov, S., Kamyshkov, Y., Zaman, T., and Schultz, D.R., J. Phys. B: At. Mol. Opt. Phys., 50 (2017) 085204.